Master's thesis

NTNU
Norwegian University of Science and Technology

Linn Bolin Haakenstad

Searching for Sources of Ultra High Energy Cosmic Rays with a Clustering Analysis of arrival directions

Master's thesis in Physics
Supervisor: Foteini Oikonomou
Co-supervisor: Domenik Ehlert
June 2024

NTNU
Norwegian University of
Science and Technology

Linn Bolin Haakenstad

Searching for Sources of Ultra High Energy Cosmic Rays with a Clustering Analysis of arrival directions

Master's thesis in Physics
Supervisor: Foteini Oikonomou
Co-supervisor: Domenik Ehlert
June 2024

Norwegian University of Science and Technology

NTNU
Norwegian University of
Science and Technology

NTNU

Kunnskap for en bedre verden

Department of Physics

FY3900 - Physics Master Project

Searching for Sources of Ultra High Energy Cosmic Rays with a Clustering Analysis of arrival directions

Author:
Linn Bolin Haakenstad

Supervisor:
Foteini Oikonomou

Co - Supervisor:
Domenik Ehlert

Date: 01.06.2024

Acknowledgements

I am grateful to everyone who has supported and guided me throughout my master's thesis journey.

First and foremost, I thank my supervisor, Professor Foteini Oikonomou, for her support and for allowing me to work on such an interesting topic.I would also like to mention Domenik Ehlert. His encouragement and help have been extremely helpful throughout my master's. His advice and help have been very useful, and I have learned a lot over the past year.

I would like to extend my thanks to Elise Lindegaard Hanssen, my fellow master's student. We have shared this journey, and her support has been invaluable. She has been a great help in discussing my thesis and offering encouragement along the way. I also want to give a special mention to Oda Hjemli and Ellen Haltuff for all the fun adventures we've shared since our first day at university. Your support and friendship have made this journey memorable and enjoyable in every way.

Special thanks go to all my fellow students at C4. Your support has made my time on campus enjoyable, and I will miss the fun and adventurous days we spent together.

Lastly, I wish to thank my family for their support. Your encouragement throughout my childhood for my interest in physics and the big questions in life has made me curious and driven to pursue this path.

Abstract

Ultra high energy cosmic rays(UHECR) are particles with energies above 10^{18}eV and are assumed to come from extra-galactic sources [1]. From the discovery of cosmic rays, one has wondered how these particles are accelerated to these extreme energies and which sources have the power to fuel this acceleration process. There are still no confirmed UHECR producers.

UHECRs arrive at Earth, and using event data from large-scale observatories makes their arrival direction and energy possible to determine. Due to the magnetic fields inhabiting the Universe, the trajectories of UHECRs are deflected as they propagate to Earth. This thesis will conduct a multiplet search on a set of simulated UHECR arrival directions, where the magnetic fields have been accounted for. The multiplet formalism will compare arrival directions and energies of UHECRs with reconstructed source directions. This will determine if it is possible to distinguish a simulated source from a simulated background. A clustering analysis will also be performed on the simulated cosmic rays using the reconstructed source directions.

This simulation showed that a source must be strong to be detected for lower declinations. Applying this analysis to a real dataset, such as the most energetic events observed by the Pierre Auger Observatory, is possible.

Sammendrag

Ultra-høyenergiske kosmiske stråler (UHEKS) er partikler med energier over 10^{18} eV, og antas å komme fra ekstragalaktiske kilder [1]. Siden oppdagelsen av kosmiske stråler har man undret seg over hvordan disse partiklene akselereres til slike ekstreme energier, og hvilke kilder som har kraften til å drive denne akselerasjonsprosessen. Det finnes fortsatt ingen bekreftede UHEKS-tilvirkere.

UHEKSer ankommer Jorden, og ved å bruke observatorier som tar opp et stort bakkeareal, er det mulig å bestemme deres ankomstretning og energi. På grunn av magnetfeltene som finnes i universet, blir UHEKSenes baner avbøyd når de beveger seg mot Jorden. I denne avhandlingen vil en multiplett-søk bli gjennomført på et sett av simulerte UHECR-ankomstretninger, hvor magnetfeltene er tatt i betraktning. Multiplett-formalismen vil sammenligne ankomstretninger og energier av UHECR med rekonstruerte kilde-retninger, for å se om det er mulig å skille en simulert kilde fra en simulert bakgrunn. I tillegg vil en klyngeanalyse bli utført på de simulerte partiklene ved bruk av de rekonstruerte kilde-retningene.

Simuleringsresultatene indikerte at ved lavere deklinasjoner må en kilde være omtrent 18% av den simulerte bakgrunnen for å bli oppdaget. Å anvende denne analysen på et virkelig datasett er mulig. Slik som de mest energiske hendelsene observert av Pierre Auger-observatoriet.

Table of Contents

List of Figures

Chapter 1

Introduction

Cosmic rays are energetic, charged particles that originate from outside the Earth's atmosphere [1]. They were first observed in 1912 by Victor Hess when he conducted an experiment measuring the radiation with increasing altitude; this ultimately gave him the Nobel Prize in physics in 1938 [2]. In 1962, cosmic rays with energies above $E > 10^{18}\,\mathrm{eV}$ [3] were observed for the first time. These particles are called ultra-high energy cosmic rays (UHECRs) and are believed to originate from extra-galactic sources [1]. Although limited information is available about these cosmic rays, several prominent theories exist regarding their production and source candidates. This topic will be further explored in Chapter 3. This thesis will look at the most energetic events and try to link the arrival directions with potential sources.

Although UHECRs were first discovered in 1962, the recurrence of highly energetic events remains low [1]. The flux of cosmic rays with energies above $4 \cdot 10^{19}\,\mathrm{eV}$ is highly suppressed [4]. A detailed discussion on the potential mechanisms responsible for this phenomenon is presented in Sec. 4.2. One primary factor for this suppression is likely the interaction with cosmic microwave background (CMB) photons. Another issue when studying cosmic rays is the deflection of the particles in magnetic fields. As they propagate through space, the particles experience deflection in the extra-galactic magnetic field (EGMF) and the galactic magnetic field (GMF). Therefore, the arrival direction of the cosmic rays may not point directly towards the source. Modelling the EGMF is challenging due to the limited information about the field. However, an upper limit for the average field strength is set at $10^{-9}\,\mathrm{G}$. The field strength can be even higher in certain regions, such as galaxy clusters and the interstellar medium, reaching up to $10^{-6}\,\mathrm{G}$. The EGMF contributes to a lower deflection of the UHECRs than the GMF, which has a strength of order $10^{-6}\,\mathrm{G}$ [1]. Particles with higher *rigidities* will be less deflected in magnetic fields. Rigidity measures how much a particle with energy E and charge Z is deflected in a magnetic field B. The mathematical definition of rigidity is $R = pc/(Ze)$ [5], where p represents the momentum of the cosmic ray, Z denotes the atomic number of the cosmic ray, whereas c is the speed of light and e is the electric charge constant. Since rigidity depends on the particle's charge and energy, rigidity is crucial when looking at particle behaviour in magnetic fields. At larger rigidities, particles are less deflected in magnetic fields. Therefore, higher rigidity events are more relevant

for examining anisotropies when studying arrival directions, as these particles will have more densely concentrated arrival directions.

Searching for correlations with catalogued sources may give insight into what sources fuel the production of UHECRs. Prominent sources such as active galactic nuclei (AGNs), gamma-ray bursts (GRBs) and tidal disruption events (TDEs) could be candidates for the acceleration of these particles [1]. Why these sources may be potential sources will be discussed further in Sec. 3.2. Sources of UHECR production have not yet been observed, and there are still many unanswered questions concerning the sources. Do these particles stem from a large number of sources? Lastly, is the maximum energy now observed at Earth the maximum energy possible for sources to inject into the acceleration process?

As an attempt to deepen the understanding of the most energetic UHECR events, observatories like the Pierre Auger Observatory(Auger) [6] and Telescope Array(TA) [7] have been constructed. When the cosmic rays hit the outer layer of the atmosphere, they interact with the molecules and create air showers. The depth of the shower maximum, $X_{\max}$, can be measured using fluorescence detectors. The depth of the shower maximum is related to the composition of UHECRs [8]. The observatories have detected incoming air showers through fluorescent detectors and Cherenkov water tanks. They have detected events in the highest energy regime, giving more insight into their composition, arrival directions, and spectrum. This data can be used to search for potential sources of these particles.

Several methods have been developed to determine potential source directions by employing theoretical models of magnetic fields, energy loss, and data from cosmic ray observatories [9]. This thesis will examine one of these methods: to look for multiplets [10]. The method is constructed by looking at events within a region of the sky and finding pairwise correlations between the cosmic rays' energies and arrival directions, assuming the cosmic rays stem from the same source. The method will be described in more detail in Chapter 5. In short, one assumes that the arrival direction of the most energetic cosmic ray will lie closer to the source direction than less energetic cosmic rays. Once all the source directions have been calculated, clustering analysis will be used to assess whether there are any patches of the sky characterized by a higher density of source directions. This analysis will be performed on different scenarios, such as only background UHECRs and background and a source. This analysis aims to find how to distinguish a modelled source from background simulations. The result of this analysis will be presented in Chapter 6.

Chapter 2

Ultra High Energy Cosmic Rays

2.1 Spectrum

The cosmic ray spectrum is constructed from observed cosmic-ray events, showing how the flux of incoming cosmic rays relates to their energies. High-energy events are detected through air-shower observations using large ground-based observatories and telescopes. In contrast, lower-energy events are detected directly using satellites like AMS-02 [11]. Lower-energy events occur more frequently and are more extensively documented than higher-energy events. The all-particle spectrum can be approximated to a power law describing incoming particles' differential flux without distinguishing their species [12]. The fitted power law is given by,

$$\frac{dN}{dE} \propto E^{-\gamma} \tag{2.1}$$

where N is the number of incoming cosmic rays, E is the corresponding energy, and γ is the spectral index [13]. The spectrum can be broadly divided into three regions, as shown in Fig. 2.1. The lower energy range, spanning from 10^{10} eV to 10^{14} eV, has a spectral index characterized by $\gamma \approx 2.7$ [1]. Galactic cosmic rays dominate this part of the spectrum. The next part of the spectrum, known as the *knee*, is located at $3 \cdot 10^{15}$ eV with the spectral index changes to $\gamma \approx 3.1$ [14]. As seen in Fig. 2.1, the number of incoming events drops drastically at energies around the *knee*. The *ankle*, probably represents the transition from galactic to extra-galactic cosmic rays, where particles have energies above $4 \cdot 10^{18}$eV [1, 14]. The highest energy observed is $166 \pm 13 \cdot 10^{18}$ eV [15]. For ultra-relativistic energies such as these, the particles have low event statistics. The knowledge of the species and sources is still, to some degree, unknown. However, there is a common assumption that the particles must originate from extra-galactic sources [1]. At these ultra-relativistic energies, cosmic rays are not thought to be confined within the magnetic field of our Galaxy [16]. In 1966, the idea of an upper limit on the energies of the ultra-high energy protons was introduced by Greisen [17], Zatsepin [18], at $5 \cdot 10^{19}$ eV as a result of cosmic-ray protons interacting with the background CMB photons. Events have been observed above this limit, though the composition of these events is not certain. It is also worth mentioning that the cut-off observed in the cosmic ray

spectrum may not be due to the propagation losses. Heavier nuclei will also undergo photo-disintegration [19], which also causes energy losses. These propagation effects will be further discussed in Sec. 4.2. Additionally, it should be mentioned that the cut-off observed in the spectrum may also stem from the inability of the source candidates to accelerate cosmic rays to higher energies.

2.2 Composition of Cosmic Rays

The overall composition of cosmic rays is not fully understood. However, measurements on the depth of the shower's maximum incoming shower relate to the mass of the primary cosmic ray [8]. For energies below 10^{10} eV the composition is well documented [20]. For these energies, protons dominate the observed events [1]. Heavier nuclei become more prominent for energies above 10^{15} eV [1]. The composition is poorly understood for energies above the *ankle* due to the limited number of events at these high energies. However, observations from Auger show that the composition is dominated by heavier nuclei at energies above $10^{18.3}$ eV [21].

Measuring, $X_{\max}$, of an incoming air shower probes the composition of the primary cosmic ray [22]. The relation between the depth of the shower and the species of the incoming cosmic ray $X_{\max} \propto \ln(\mathrm{E}_0/\mathrm{A})$, where A atomic number of the primary cosmic ray [22].

The observed flux indicates that the heavier nuclei dominate the higher energy regime, though this is still not yet confirmed.

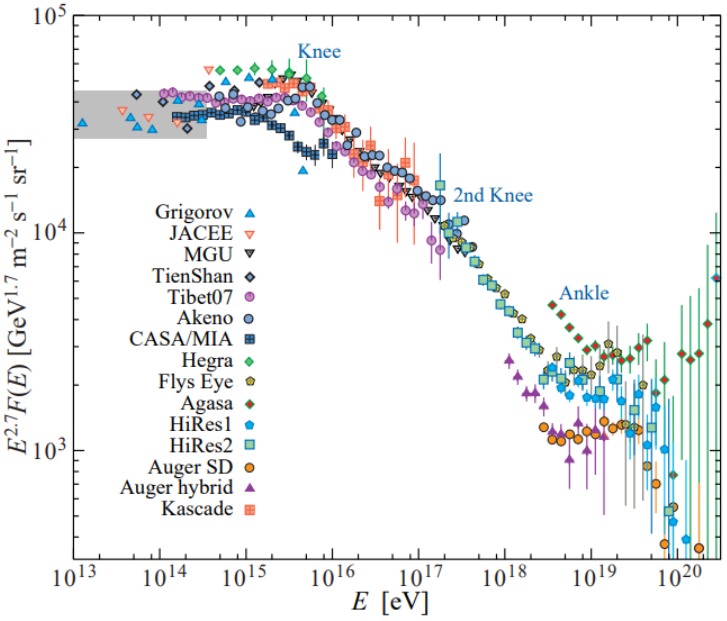

Figure 2.1: The Cosmic Ray spectrum, taken from the article [23].

2.3 Arrival Directions

As charged particles, UHECRs are deflected by magnetic fields during their propagation. They travel through both extra-galactic and Galactic magnetic fields, contributing to their trajectories' dispersion. In addition to this dispersion, they also experience energy loss. The effects of magnetic fields and collisions with background photons, such as those from the CMB and the extra-galactic background light (EBL), will be further discussed in Chapter 3. This thesis will explore methods to link the arrival direction with the potential source direction in Chapter 5, considering magnetic fields and observed energies. Linking the arrival direction with existing catalogued extra-galactic sources can enhance searching for possible cosmic-ray sites. Additionally, correlating the arrival directions of cosmic rays can further aid in identifying these sites. Large-scale anisotropies have been discovered. It is also worth mentioning that these anisotropies do not necessarily point towards any known source candidates and there has not yet been discovered an acceleration source of UHECRs.

The Auger collaboration has conducted comprehensive studies on the correlation between the energies and arrival directions of UHECRs [24, 25]. Their findings indicate a significant large-scale anisotropy, characterized by a dipole amplitude of $6.5^{+1.3}_{-0.9}\%$ in the direction of $\alpha = 100° \pm 10°$ and $\delta = -24^{+12}_{-13}°$ for UHECRs above $8 \cdot 10^{18}$eV [26]. This anisotropy suggests the presence of high-energy sources nearby but does not point to any specific ones.

Looking at energies above $4 \cdot 10^{19}$ eV, they found a potential higher density of arrival direction that may point towards strong catalogued sources [27]. Centaurus A (Cen A) is a strong radio source that may provide an environment for UHECR acceleration.

Cen A is a promising source as a possible UHECRs emitter. However, the observations may also indicate an excess of UHECRs in the direction of starburst galaxies, such as NGC 4945 [27].

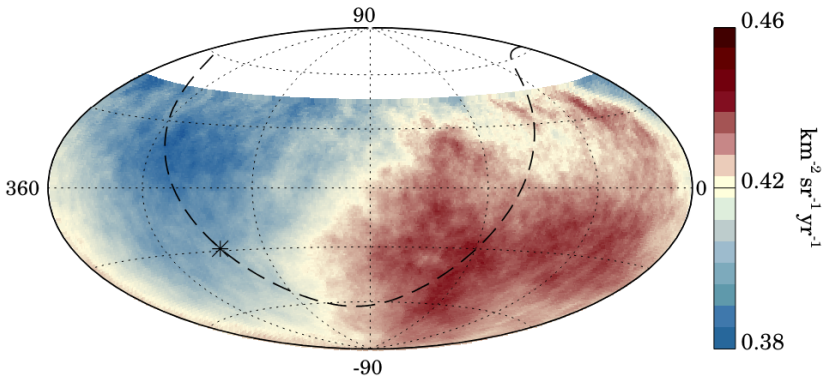

Figure 2.2: Dipole anisotropy observed by Auger plotted in an equatorial projection. Taken from the [26]

2.4 Detection

The detection of UHECRs is done by large ground-based observatories, mostly due to the low event statistics. The measurements give an insight into the arrival direction, incoming energy and composition of cosmic rays.

Pierre Auger Observatory

Pierre Auger Observatory is a hybrid detector in Mendoza, Argentina [28]. Location of the Observatory is given here in terms of position in latitude and longitude, (69°W, 35°S, 1400 m a.s.l.) [29]. The observatory has been collecting data from 2004 until 2021. The observatory is fully exposed to the Southern Hemisphere due to its location. The exposure of the observatory depends on observational concentration due to the rotation of the Earth [30].

Surface Detector: The Observatory consists of 1660 surface detector stations with 1500 m spacing between each station. They are placed in a triangular grid [31]. These detectors are water Cherenkov detectors. The diameter of each tank is 3.6 m, and it contains three photomultipliers to detect Cherenkov light. These water tanks are filled with purified water, with a water depth of 1.2 m. The number of detected cosmic rays are improved by covering such a large surface area with Cherenkov detectors.

Fluorescence detectors: The observatory consists of fluorescent telescopes. The atmosphere works as a fluorescence material due to the nitrogen. The detectors capture ultraviolet (UV) emission produced when cosmic rays interact with nitrogen. During this process, the molecules de-excite and emit photons in the UV range [31].

Chapter 3

Sources and Acceleration

3.1 Acceleration Processes

The acceleration mechanisms of UHECR are not yet well understood. For these acceleration processes to be considered efficient, they must align with the observed cosmic-ray flux. In this thesis, the discussion of these mechanisms is categorized into two distinct methods of acceleration [32]. The first method involves the transfer of energy from a macroscopic environment to microscopic particles. The second method concerns charged particles moving through a magnetic field, which induces an electric field that accelerates the particles to high energies [32].

The initial method uses a stochastic process in which particles are confined within an acceleration region, gaining energy through repeated crossings of the shock front. Magnetic inhomogeneities provide the particle with a possibility of scattering the particle back and forth with the probability of $(1 - P_{\mathrm{esc}})$ [32]. Enrico Fermi first defined this mechanism in 1949 [33].

The probability of a particle staying within the acceleration region is given by $(1 - \mathrm{P_{esc}})$. The particle will cross the shock front n times. For each crossing, the particle gains an energy of $\mathrm{d}E$, which depends on the direction in which the particle crosses the shock. After n crossings, the probability of the particle staying within this region is given by $(1 - \mathrm{P_{esc}})^n$. When summing over all the crossings, the number of particles confined within the region long enough to be accelerated to energies above E naturally follows a power law,

$$\mathrm{N}(>\mathrm{E}) \propto \frac{1}{\mathrm{P_{esc}}} \left(\frac{\mathrm{E}}{\mathrm{E_0}} \right)^{-\gamma} \tag{3.1}$$

which is desired due to the observed flux of the incoming cosmic rays [1].

The Fermi acceleration method uses the change of reference system to describe the energy gain of the particle. A particle with initial energy E_{in} will in the rest frame of the moving cloud have the energy,

$$E_{\mathrm{in}} = \Gamma \, E_{\mathrm{in}} \, (1 - \beta \cos\theta_{\mathrm{in}}) \tag{3.2}$$

Where $\beta = V/c$ is the velocity of the moving cloud.

Fermi first introduced the concept of second-order acceleration in his 1949 paper [33]. In regions with high-intensity moving magnetic field lines, a particle will gain energy if it encounters the field head-on and is ejected forward. However, if the particle is ejected backwards, it will lose energy. Overall, the net energy gain is positive because head-on collisions occur more frequently than instances where particles overtake the clouds. The average relative energy gain can be expressed as [1],

$$\frac{\langle \Delta E \rangle}{E_{\text{in}}} = \frac{1 - \beta \cos\theta_{\text{in}} + \beta \cos\theta'_{\text{out}} - \beta^2 \cos\theta_{\text{in}} \cos\theta'_{\text{out}}}{1 - \beta^2} - 1 \tag{3.3}$$

where the subscript "*in*" and the subscript "*out*" corresponds to the outgoing particle. In addition, the θ' represents the angle in the rest-frame of the moving cloud, while θ is the angle in the lab-frame. For encounters with plasma clouds, the incoming angle is averaged over the angles 0 and π. The fractional energy gain per encounter can be expressed as $\xi = \Delta E/E$ by inserting the averaged angles; this is the relation for the particle's encounter with the plasma clouds.

$$\xi = \frac{1 + \frac{1}{3}\beta^2}{1 - \beta^2} - 1 \sim \frac{4}{3}\beta^2 \tag{3.4}$$

which is derived from equation (12.13) in [1], by taking the angular average for each encounter for both the incoming (θ_{in}) and outgoing (θ_{out}) angles. The average of the outgoing particle is, $\langle \theta'_{\text{out}} \rangle = 2/3$, due to interactions with plasma clouds. For the incoming angle, $\langle \theta_{\text{in}} \rangle = -2/3$. This velocity gain is called *Fermi second-order acceleration* because the average energy gain per interaction scales with $\sim \beta^2$.

Diffusive Shock Acceleration

Diffusive shock acceleration(DSA) occurs when charged particles are accelerated in a planar shock front [1]. The acceleration process obtained in DSA is *the Fermi first order acceleration.*

In *Fermi first-order acceleration*, the average incoming angle is set to zero, in contrast to *Fermi second-order acceleration.* The averages over incoming and outgoing angles are due to the particles moving upstream and downstream with respect to a shock wave. The outgoing angle average is $\langle \theta_{\text{in}} \rangle = -V/3$, where V is the velocity of the shock. This gives,

$$\xi = \frac{1 + \frac{1}{3}\beta^2}{1 - \beta^2} - 1 \sim \frac{4}{3}\beta \tag{3.5}$$

a linear energy gain. This type of acceleration must be the primary acceleration mechanism in shocks.

DSA can occur in both relativistic shocks and non-relativistic shocks [34]. In non-relativistic shocks, $v_{\text{CR}} >> v_{\text{sh}}$, the cosmic rays gains energy by crossing the shock front many times and when reaching high enough energies, escaping the acceleration region. Some papers have speculated that acceleration of UHECR in ultra-relativistic shocks is probably not possible because this would create a steeper spectrum of UHECR than now observed [35], though acceleration in mildly-relativistic

shocks may occur. The DSA gives a power-law spectrum of $\gamma \simeq 2$, consistent with cosmic-ray observations [36].

Magnetic Reconnection

Magnetic reconnection happens when magnetic field lines cross and then break up and reconnect. This process is most commonly seen in solar flares. Accelerating cosmic rays through magnetic reconnection can arise in highly magnetized AGN jets or GRB jets [37].

Shear Acceleration

Shear is a form of stress and friction between two media. A shear shock can be modelled as two flows with different velocities moving in parallel. In AGN jets, shear acceleration may occur when the spine of the jet moves with a significantly higher velocity than the outer layer [38].

3.2 Constraints on Candidate Sources

For the acceleration of the UHECRs to be feasible, the possible source candidates need to satisfy some theoretical conditions. In addition, the sources must be relatively close due to the energy loss that occurs as cosmic rays travel through space to reach the Earth.

Hillas Condition

The Hillas condition is a geometrical condition for a source to confine the particles long enough to gain ultra-relativistic energies [12]. Mathematically, this constrain can be expressed as,

$$\epsilon_{max} = R\,B\,q \tag{3.6}$$

where β is the velocity of the shock, q is the charge of the nuclei, R is the radius of the acceleration region and B is the average magnetic field [30]. The principle behind the Hillas condition is that the acceleration region must be larger than the Larmor radius ($r_L = \gamma m \beta / B|q|$) of the particle in the magnetic field. The relation between the magnetic field and the radius of a source can be plotted against each other in a logarithmic plot, seen in Fig. 3.1.

The Blandford condition

The Blandford condition is a restraint on the minimal luminosity to accelerate UHECRs [39]. The theoretical limit is derived for charged particles in an electric field, assuming a vacuum between the induced fields. For protons of energies $10^{20}\,\mathrm{eV}$,

$$L \geq 3 \cdot 10^{42} \mathrm{erg\,s^{-1}} \frac{\Gamma^2}{\beta} \left(\frac{(E/Z)}{5 \cdot 10^{18}\,\mathrm{eV}} \right)^2 \tag{3.7}$$

This is called the Blandford condition due to his proposal for a minimum power needed by a source to accelerate particles up to ultra-relativistic energies [40].

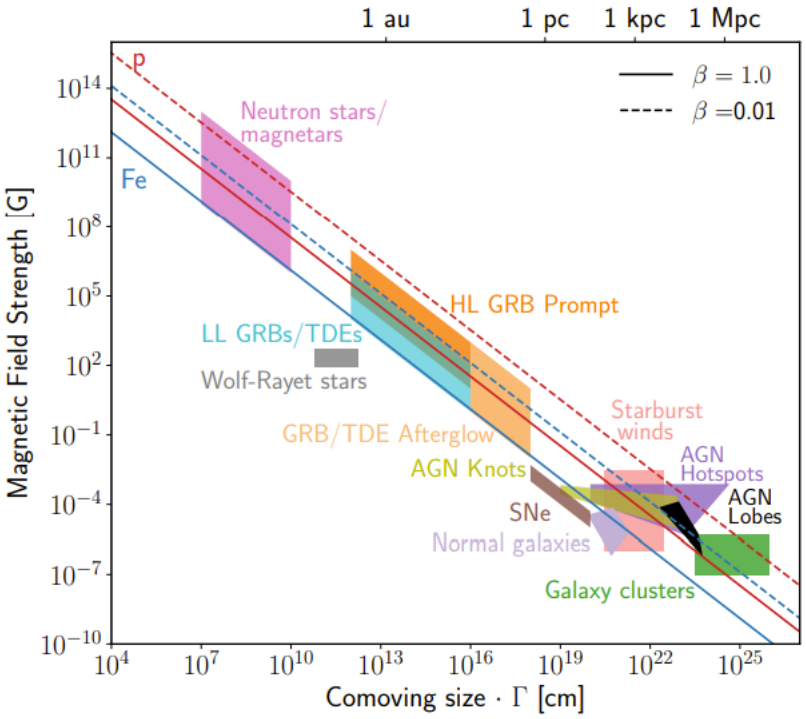

Figure 3.1: The graph depicts the Hillas plot. The plot shows the linear relationship between the magnetic field's strength and the acceleration site's radius. The lower blue line shows the minimum requirement for accelerating iron, and the red dotted line shows the same for protons. All sources depicted above the lines may be prominent sources for UHECR acceleration. The plot is taken from [30].

3.3 Potential Sources

Active Galactic Nuclei

An active galactic nucleus (AGN) is a highly luminous engine in the centre of a galaxy [41]. The AGN is powered by gravitational potential energy, which fuels an accretion disk surrounding the supermassive black hole [1]. AGNs have traditionally been divided into two sub-classes, *radio-loud* and *radio-quiet* [42]. Radio-loud AGNs are usually accompanied by a jet. A jet can form along the spin axis of the accretion disk [1]. Jetted-AGNs have been considered a potential source for UHECRs production [43] due to the large acceleration region and the high luminosity. This implies that the source may be strong enough to inject the energy needed for acceleration to ultra-relativistic energies. AGNs with mildly relativistic shocks are possibly more prominent for cosmic ray acceleration than ultra-relativistic shocks [43]. Jetted-AGNs are a well-known source for several mildly relativistic shocks in the back-flow region of a jet [43]. In these regions, diffusive shock acceleration may occur [43]. As mentioned in Sec. 2.3, Cen A may be a potential source for UHECR acceleration and is a radio-loud AGN with an accompanying jet. The source lies approximately 3-4 Mpc away from the Earth [44].

Gamma Ray Bursts

Gamma-ray bursts (GRBs) are highly energetic electromagnetic events discovered in 1966 by U.S. military satellites [45]. GRBs are classified as short bursts, which may occur from binary neutron star mergers, and long bursts, possibly due to a (Super Nova (SN)) core-collapse forming a black hole [46]. Jets may arise in environments close to these black holes. These environments have high radiation pressure, which causes matter to move with velocities close to the speed of sound in the medium through which the shock traverses. In these environments, cosmic rays may be accelerated to ultra-relativistic energies [47]. The confinement region's radius in GRBs is not as big as for AGN but still satisfies the Hillas condition mentioned in Sec. 3.2 due to strong magnetic fields. Low-luminosity GRBs are perceived as a more probable source for UHECR acceleration due to a higher event rate than the High-Luminosity GRBs [48].

Tidal Disruption Events

Tidal disruption events(TDEs) are events where the gravitational pull from a supermassive black hole disrupts a star. Some TDEs have been observed with a relativistic outflow. The fast outflow may accommodate good conditions for cosmic ray acceleration [49]. Some of the observed jetted-TDEs satisfy the Hillas condition [50] and the Blandford condition as these sources can be very luminous [49].

Other Candiate Source

Shocks in galaxy clusters, non-jetted AGNs, and pulsars may also be potential sites for UHECR acceleration. Shocks can occur around galaxy clusters, and the acceleration regions in these environments usually satisfy the Hillas condition. Non-jetted AGNs have strong winds that may create suitable environments for UHECR acceleration [51]. Pulsars, with their strong magnetic fields, seem to provide conditions that satisfy the Hillas criterion for UHECR production.

Chapter 4

Propagation

4.1 Magnetic Fields

The propagation of UHECRs is affected by magnetic fields. A charged particle in a magnetic field moves in a circular motion perpendicular to the magnetic field lines. The radius of this circular motion is defined as the Larmor radius; the mathematical definition can be found in Sec. 3.2. The deflection of the trajectory of a particle in the magnetic field can be described using the Larmor radius and the particle's rigidity. For small angle approximations, $\theta \approx l_{\mathrm{coh}/R_L}$, where l_{coh} is the coherence length and R_L is the Larmor radius of the particle's movement along the magnetic field lines. For a particle travelling a distance d, the number of steps can be defined as $N \approx d/l_{\mathrm{coh}}$. To get the total deflection accounting for all steps,

$$\langle \theta^2 \rangle \approx N \cdot \frac{4}{9} \cdot \left(\frac{l_{\mathrm{coh}}}{R_L} \right)^2 = \frac{4}{9} \cdot \frac{d}{l_{\mathrm{coh}}} \cdot \left(\frac{l_{\mathrm{coh}}}{R_L} \right) = \frac{4}{9} \cdot \frac{d\, l_{\mathrm{coh}}}{R_L^2} \tag{4.1}$$

where the 4/9 comes from assuming a diffusive behaviour of the cosmic rays. The root mean square of the angular deflection along the line of sight can be expressed as [1],

$$\theta_{\mathrm{RMS}} = 3.5^\circ \left(\frac{Z\, B}{10^{-9}\, G} \right) \left(\frac{10^{20}\,\mathrm{eV}}{E} \right) \left(\frac{d}{100\,\mathrm{Mpc}} \right)^{\frac{1}{2}} \left(\frac{l_{\mathrm{coh}}}{1\,\mathrm{Mpc}} \right)^{\frac{1}{2}} \tag{4.2}$$

extracted from the small angle approximation where $\delta\theta \approx d/R_L$. Applying a random walk process to model the behaviour of particles in magnetic fields is essential due to the limited knowledge about the magnetic field strength and the particles' trajectories. Understanding the behaviour of these particles within the galactic and extra-galactic fields is crucial for comprehending their origins. Since UHECRs are most likely of extra-galactic origin, the particles will be affected by both an EGMF and a GMF. The information about the GMF is more extensive than that about the EGMF.

Galactic Magnetic Field

The galactic magnetic field (GMF) affects the trajectories of cosmic rays. The GMF is significantly more potent than the EGMF. The GMF has an average strength of

approximately $3\,\mu$G [1]. The Milky Way is a spiral galaxy, and the structure of the GMF likely mirrors the structure of the Milky Way [52]. Modelling the GMF is complicated because the observations are taken from Earth inside the field, making the overall structure hard to map. There have been several attempts at constructing a galactic magnetic field model; in Fig. 4.1, some of the models are presented. Jansson and Farrar developed one of the most prominent models in 2012 [53].

Jansson and Farrar's model: This model assumes that the galactic magnetic field is divided into three structures. Large-scale coherent, striated, and small-scaled turbulent fields make up the overall structure of the modelled field.

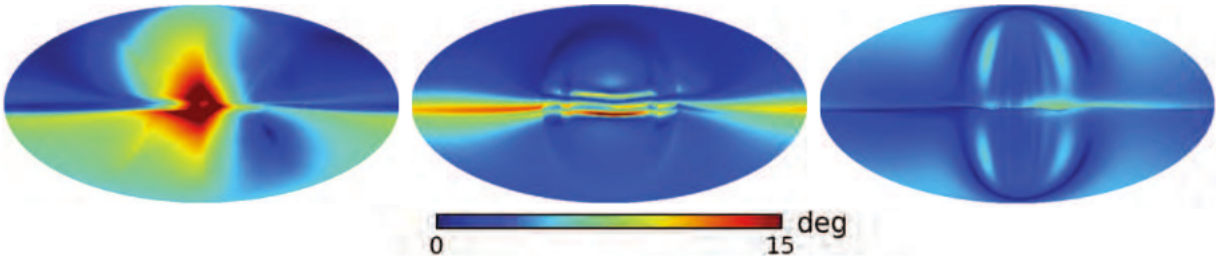

Figure 4.1: Magnetic field models, describing three different numerical models describing deflection of a $6 \cdot 10^{19}$ eV proton the GMF. The first model from the left is the JF12 model, the second is the SR10, and the third is the PTK11 model. Each model describes the large-scale galactic magnetic field. Taken from the paper [54]

From a recent paper by Unger et al. [55], a new model of the GMF is presented. This model focuses on the two observable: Rotation measures and the polarised intensity. Rotation measures are obtained from extra-galactic polarized radio sources. The polarized intensity is measured by observing our Galaxy's synchrotron emission from cosmic-ray electrons. Predicted deflection angle for is $\sim 5^\circ$ for ultra-high energy protons with energies $6 \cdot 10^{19}$ eV [1].

Extragalactic magnetic field

The upper limit on the average strength of the EGMF is set as 10^{-9} G, by looking at Faraday rotation measurements of distant quasars [56]. The effect of the EGMF on UHECRs can still be prominent; the EGMF can have a stronger and more turbulent component in galaxy clusters. The strength can become as large as 10^{-6} G with a coherence of $l_{coh} \sim 100\,\text{kpc}$ [1]. The uncertainty of the EGMF is vast. Only a little is known of the EGMF, but there are two prominent theories of how the field has come to exist. The **primordial** theory assumes that the field has been generated by a seed field produced in the early Universe and then amplified by cosmological processes that took place early on in the universe [30]. The second theory, **the astrophysical**, assumes that astrophysical processes feed the EGMF.

To compare the deflection angle of the EGMF with the GMF, consider a 10^{20} eV proton traversing a turbulent field with a strength of 10^{-9} G and a coherence length of 100 kpc, and then compare this scenario with its traversal in the GMF. Inserting the values for the EGMF in Eq. 4.2 gives a deflection of $\simeq 0.15^\circ$ [57]. Compare to a deflection of $\simeq 3.5^\circ$ in the GMF.

4.2 Energy loss

As explained in Sec. 4.1, high-energy cosmic rays may point more directly to their sources than lower-energy cosmic rays, as they experience less deflection in magnetic fields. However, as cosmic rays experience higher energies, they are more prone to energy losses. This section will investigate how cosmic rays are affected by these mechanisms and how the theoretical models for the energies fit the experimental data observed. This thesis will take a look at four main energy loss processes.

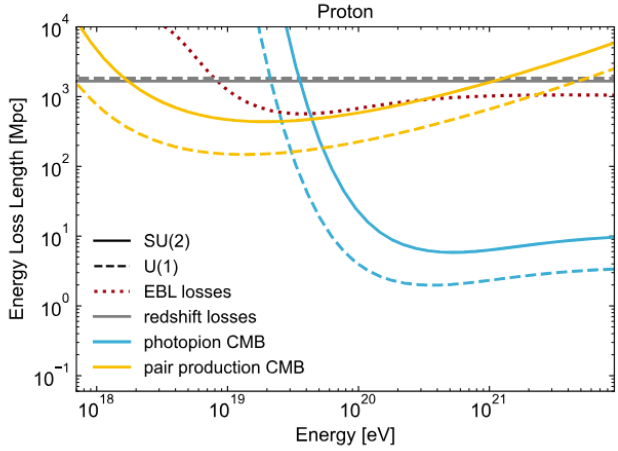

(a) Proton energy loss

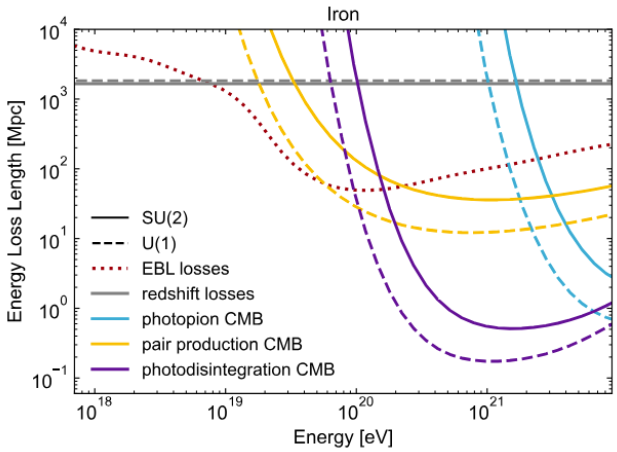

(b) Iron Energy Loss

Figure 4.2: The graphs show the energy loss length of a (a) proton and (b) iron nucleus for each energy regime. The redshift loss is constant and is not affected by the energy of the cosmic ray. Taken from [58].

Photon Fields

The cosmic rays interact with the CMB photon field and the EBL as they traverse through space. The interactions with the background photons cause the cosmic rays to lose energy. The CMB photon field is a consequence of the dense and hot beginning of the Universe. As the Universe expanded, the radiation cooled, forming the CMB photon field observed today [59].

The EBL consists of the accumulated light emitted by all sources in the Universe since its beginning. It spans the electromagnetic spectrum from the infrared to the ultraviolet [60].

Adiabatic energy loss

UHECRs experience energy loss due to the expansion of the Universe [61]. The rate of energy loss for one cosmic ray is given by

$$E \cdot \left(\frac{\mathrm{d}\,E}{\mathrm{d}\,x}\right)^{-1} = \frac{c}{H(z)} = \frac{c}{H_0} \cdot \frac{1}{\sqrt{\Omega_M + (1+z)^3\,\Omega_\Lambda}}$$

where z denotes the redshift, H_0 is the Hubble constant with a value of $H_0 = 75\,\mathrm{km\,sec^{-1}\,Mpc^{-1}}$, $\Omega_M \approx 0.3$ represents the density of baryonic matter, and $\Omega_\Lambda \approx 0.7$ represents the density of dark energy [62, 63]. This energy loss mechanism is only relevant for cosmic rays which traverse cosmological distances [64] and is the dominant process for protons with energies $E \lesssim 2 \cdot 10^{18}\,\mathrm{eV}$ and for heavier elements $E/A \lesssim 2 \cdot 0.5^{18}\,\mathrm{eV}$ [65]. From Fig. 4.2, the energy loss due to redshift is not related to the energy of the cosmic ray, which means that the energy loss rate only depends on the distance from the source to the Earth.

Photopion production process

When ultra-relativistic protons interact with a CMB or EBL photon, they produce mesons (specifically pions). This process is the primary mechanism behind the theoretical limit suggested by Greisen–Zatsepin–Kuzmin for suppressing protons [66].

$$p + \gamma \to \Delta^+ \to \begin{cases} n + \pi^+ \\ p + \pi^0 \end{cases}$$

The primary decay channel for $\pi^+ \to \mu^+\nu_\mu \to e^+\nu_e\nu_\mu\bar{\nu_\mu}$. The neutron does decay further, $n \to p + e^- + \bar{\nu_e}$, resulting in a proton, electron and an anti-electron neutrino. For the neutral pion, the primary decay mode is $\pi^0 \to 2\gamma$. The mass of the Δ^+-meson is $m_\Delta = 1232\,\mathrm{MeV}$, and is the minimum energy requirement for the process to occur. For heavier nuclei, some models assume a single-particle model, which presumes that a photon only interacts with one of the nuclei's nucleons and does not affect the other nucleons. The threshold energy for a head-on interaction with a CMB photon and a nucleus of mass m_N can be described as,

$$E_{\mathrm{th}}^{N,\pi} = \frac{m_\pi\,c^4\,(m_N + m_{\pi/2})}{2\epsilon} \approx 6.8 \cdot 10^{19}\,\left(\frac{\epsilon}{\mathrm{meV}}\right)\,\mathrm{eV} \tag{4.3}$$

where ϵ is the energy of the CMB or EBL photon [67]. The energy threshold is on the order of $\sim 7 \cdot 10^{19}\,(\,\mathrm{meV}/\epsilon)\,\mathrm{eV}$. This implies that for a proton interacting with a CMB photon with energy $\epsilon \approx 0.6\,\mathrm{meV}$, the threshold energy is $\sim 4 \cdot 10^{19}\,\mathrm{eV}$ [68].

Electron-Positron pair production

Electron-positron pair production occurs when lower-energy protons interact with CMB photons, producing an electron-positron pair. The energy threshold for this

process is lower than that for photopion production.

$$p + \gamma_{\text{CMB}} \rightarrow p + e^- e^+$$

Photo-disintegration

Photo-disintegration occurs when a nucleus interacts with a background CMB photon or EBL photon and is disintegrated into a less heavy particle; this is the main energy loss process for UHECR nuclei [69].

$$X_Z^A + \gamma_{\text{CMB}} \rightarrow \begin{cases} X_Z^{A-1} + n \\ X_{Z-1}^{A-1} + p \end{cases} \tag{4.4}$$

This type of interaction is dominant for the ultra-relativistic energies, and the cross-section for the process increases as the mass of the incident cosmic ray increases [70]. The threshold energy for photo-disintegration of a He-nuclei on the CMB photon occurs at energies above 10^{19} eV and for a Fe-nuclei this energy loss mechanism becomes significant at energies above 10^{20} eV [70]. Regarding the energy threshold for the photons, this process predominantly occurs for photons with energies $\epsilon \lesssim 30$ MeV [62].

Chapter 5

Methods

The primary objective of this work is to identify potential sources of UHECRs. Various approaches can be used for this purpose, including neural networks [71], thrust ratio [9], and multiplet searches [10]. This study will concentrate on the latter to correlate the arrival directions of UHECRs with possible source directions. Detailed information on UHECR simulations and how the model incorporates magnetic fields and the observatory's exposure is provided in Sec. 5.1. The procedure of the multiplet search is explained in Sec. 5.2. The clustering analysis performed on the reconstructed arrival directions is discussed in Sec. 5.3.

5.1 UHECR simulations

For the background simulation, UHECRs are distributed at random positions uniformly in the sky. This distribution of particles will act as a background simulation. Over these large distances, the small deflections cause the paths of the cosmic rays to become scrambled. Incorporating the simulated arrival directions of UHECRs in a CRPropa map involves adding cosmic rays using coordinates in right ascension and declination (α, δ). The cosmic rays are evenly distributed in α following a uniform distribution.

For δ, the distribution must account for the varying area coverage at different zenith angles. Mathematically, this is represented as $\delta \in \sin^{-1}(2P-1)$, where $P \in (0,1)$. The random distribution in declination arises from the area covered at an angle δ by the observatory. This follows a $\cos\delta$ distribution. The area change can be expressed as $\Delta A = 2\pi \cos\delta \, \Delta\delta$, implying the probability of finding a particle within ΔA is $dP \propto \cos\delta d\delta$.

The probability scaled with declination is obtained using a cumulative probability distribution, yielding $P(\delta) = 1/2(1+\sin\delta)$. This results in a declination distribution given by $\delta = \sin^{-1}(2P-1)$.

The cosmic rays are assigned energies according to a power-law distribution, $P \propto E^{-\gamma}$. Observations indicate that cosmic-ray energies follow this distribution with

a spectral index, γ. The minimum and maximum energies of the incoming cosmic rays and the spectral index must be known to assign energies using the power-law distribution. The probability of a cosmic ray having a specific energy is given by a bounded Pareto function,

$$P_E(E) = \frac{1 - E_{\min}^{\gamma} E^{-\gamma}}{1 - \left(\frac{E_{\min}}{E_{\max}}\right)^{\gamma}} \tag{5.1}$$

where P_E lies between 0 and 1. This distribution allocates the highest energies to a few cosmic rays, which is consistent with observations of ultra-high energy events if γ is positive. The distribution of energy per cosmic ray can be seen in Fig. 5.1

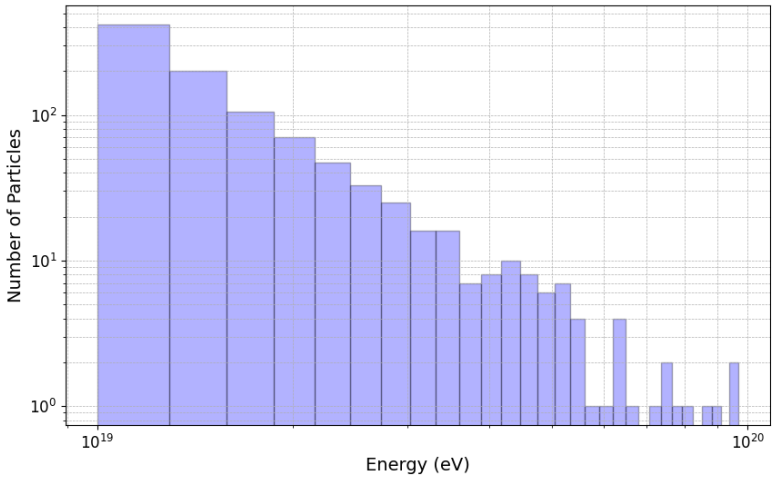

Figure 5.1: The Pareto function applied to a set of 1000 cosmic rays with the energy distribution $10^{19}\,\text{eV} < \text{E} < 10^{20}\,\text{eV}$.

A strong source is incorporated into the model by introducing cosmic rays into a specific region of the sky. The source cosmic rays are distributed according to the function $P(E, \theta) = \exp(-\theta/\theta_s^2)$, resembling a Gaussian distribution. The source cosmic rays will be added to a specific region of the sky, resulting in a higher density of cosmic rays in that area. Because of deflections in the EGMF, the source particles will be somewhat dispersed. Higher-energy cosmic rays will be less scattered compared to lower-energy cosmic rays. Consequently, the spread of the Gaussian distribution will depend on the particle's energy. The spread is represented by θ_s^2. The spread function is expressed as,

$$\theta_s^2 = 0.025^\circ \cdot Z \left(\frac{D}{\lambda}\right)^{\frac{1}{2}} \left(\frac{\lambda}{10\,\text{Mpc}}\right) \left(\frac{B}{10^{-11}\,\text{G}}\right) \left(\frac{E}{10^{20}\,\text{eV}}\right)^{-1} \tag{5.2}$$

where D is the distance traversed by the cosmic ray, λ and B is the coherence length and the strength of the magnetic field, and E is the energy of the cosmic ray moving in the magnetic field [72]. The variable Z is the atomic number. The function depends on energy. The cosmic rays with the highest energies will have a smaller deflection and, therefore, be closer to the source's fixed centre.

Applying the Magnetic lens

The next step in the procedure is to account for the galactic magnetic field that will affect the cosmic rays' arrival directions. Accounting for the GMF is done by adding a magnetic lens to the simulated cosmic rays. This lens is constructed based on the model by Jansson and Farrah 2012 and is called *JF12 regular field model*. This lens is convenient when tracing the trajectories of UHECRs because it saves computational power by not following the UHECR's trajectories through the magnetic field lines but instead using their arrival direction to map their position before entering the Milky Way. The lens consists of a series of matrices, each corresponding to different rigidities. These matrices map the arrival directions of the cosmic rays on Earth to positions on the edge of the Milky Way [73]. The lens applied to the UHECR can be seen in Fig. 5.2. The cosmic-ray distribution should appear relatively similar before and after applying the lens. However, the cosmic rays in Fig. 5.2b should show a more dispersed distribution.

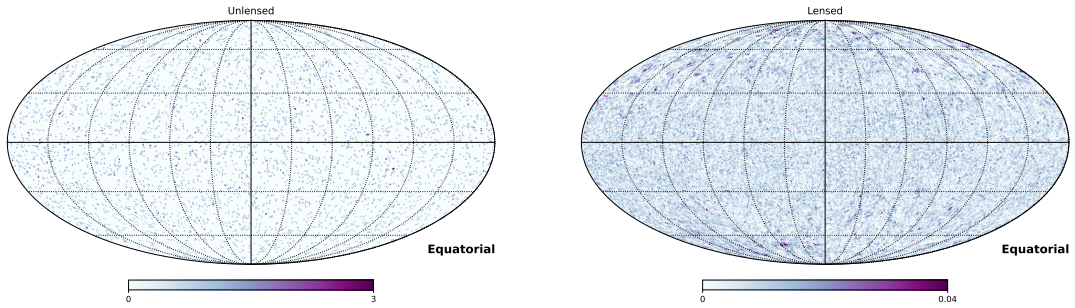

(a) Un-lensed map.

(b) Lensed map.

Figure 5.2: Isotropic distribution of cosmic rays $N = 5000$. Fig. 5.2b shows the cosmic rays are more spread out compared to Fig. 5.2a.

Accounting for the Exposure of the Pierre Auger Observatory

The next step in providing a simulation that can be applied to real observational data is to add the exposure of a chosen observatory. For this specific algorithm, the exposure of the Auger Observatory is applied to the simulated UHECRs.

The Auger Observatory has a uniform view in right ascension due to the Earth's rotation. However, the view of the declination range of the Auger Observatory is dependent on its geographical position. Since the Auger Observatory is situated south of the equator, it has a clear view of the Southern Hemisphere but can only observe cosmic rays below $\delta \sim +24.8°$ [74].

A Monte Carlo acceptance method will be used to simulate the observed flux of cosmic rays detected by the Auger Observatory. The exposure model uses, as mentioned in [75], the time-integrated effective collecting area for flux from each sky position. The exposure model given in this paper uses a constant a_0, which is the latitude for this simulation. The declination, δ, is varying between $-\pi/2$ and $\pi/2$. The variable ξ is defined by,

$$\xi = \frac{\cos(\theta_{\max}) - \sin(a_0)\sin(\delta)}{\cos(a_0)\cos(\delta)}$$

Here, $\theta_{\max}$ represents the maximum observational angle of the Auger Observatory in galactic coordinates. This value is assumed to correspond to the angle at which the observatory operates with maximum efficiency [75]. ξ is dependent on δ and corresponds to a geometrical factor that considers the position of the Auger Observatory and the arrival directions of the cosmic rays. ξ is used when calculating the maximum zenith angle, α_m,

$$\alpha_m = \begin{cases} 0, & \text{if } \xi > 1 \\ \pi, & \text{if } \xi < -1 \\ \cos^{-1}(\xi), & \text{otherwise} \end{cases}$$

determining the view of the Auger Observatory. Inserting the geographical position of the Auger Observatory $a_0 = -35°$, $\theta_{\max} = 60°$, gives a mathematical model for the sky-view of the observatory. From these values, one can find a relation with the relative exposure,

$$\omega(\delta) \propto \cos(a_0)\cos(\delta)\sin(\alpha_m) + \alpha_m \sin(a_0)\sin(\delta)$$

the expression gives a number between 0 and 1, depending on how likely it is to observe a cosmic ray in this position. The exposure of the Auger Observatory can be seen in Fig. 5.3, shown in galactic coordinates.

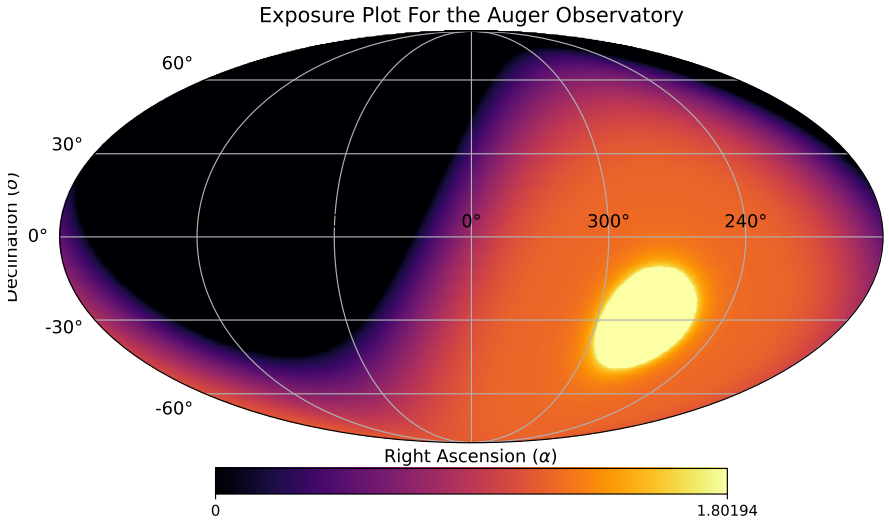

Figure 5.3: Exposure plot for the Auger Observatory plotted in galactic Coordinates.

The applied exposure of the Auger Observatory to the lensed cosmic rays can be seen in Sec. 5.1. The distribution of cosmic rays remains, isotropic in the patches of the sky that the Auger Observatory can see.

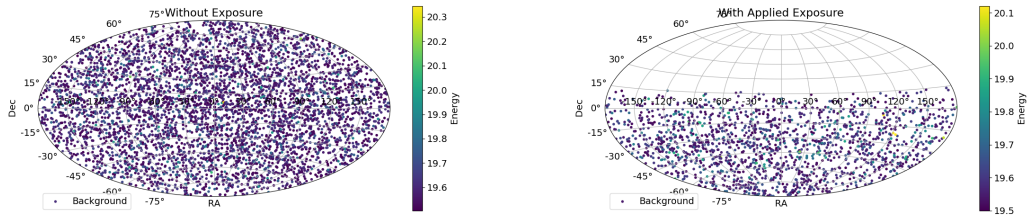

(a) Isotropic (b) Equatorial

Figure 5.4: The exposure of the Auger Observatory applied to a uniform distribution of cosmic rays.

5.2 The multiplet search

With the simulated dataset of realistic arrival directions now defined, the process of identifying source directions can be initiated. The concept behind this method is to use the arrival direction and the energies of cosmic rays to find a possible source direction [10]. The method relies on several assumptions. First, it assumes all arriving cosmic rays have the same atomic number. Second, it asserts that higher-energy cosmic rays are less deflected in magnetic fields. Finally, by analyzing the arrival directions of these higher-energy cosmic rays, it becomes possible to correlate lower-energy cosmic rays with their higher-energy counterparts. This correlation helps to identify their potential sources. It is assumed that the deflection angle between the source and the arrival direction of the cosmic ray is given by,

$$\sin\theta = \frac{Z}{E}\left(\frac{c\,e\,D\,|\vec{B}|}{2}\right) \tag{5.3}$$

where E is the energy of the cosmic ray, c the speed of light, Z the charge of the cosmic ray, B the uniform magnetic field in which the motion of the cosmic ray is perpendicular to this field, and D is the distance to the source. Now, let's assume that two cosmic rays, i and j, have the same electric charge and originate from the same source. The relation between the deflection angles and the energy can be written as,

$$\frac{\sin\theta_i}{\sin\theta_j} = \frac{E_j}{E_i} \implies \theta_j = \sin^{-1}\left(\frac{E_i}{E_j}\sin\theta_i\right) \tag{5.4}$$

where $E_i > E_j$. This relation expresses θ_j as a function of θ_i. Since the angular separation between the cosmic rays, $\Delta\theta = \theta_i - \theta_j$, is known, $\Delta\theta$, is substituted into the equation above. This results in the equation,

$$\theta_i = \sin^{-1}\left(\frac{\sin\Delta\theta}{\frac{E_i}{E_j} - \cos\Delta\theta}\right) \tag{5.5}$$

where all variables in this equation are observable and can, therefore, be used to determine a potential source direction.

To apply this method, one must identify the multiplet pair to reconstruct the source direction. In one multiplet pair, there are two cosmic rays i and j, each defined by a position and energy $(\alpha_i, \delta_i, E_i)$ and $(\alpha_j, \delta_j, E_j)$, where $E_i > E_j$. Cosmic ray i will have a smaller deflection than j. The reconstructed source direction will lie on a straight line starting from cosmic ray i, in the direction of the unit vector formed by i and j, positioned close to i.

This formalism relies on several assumptions. The first assumption is that cosmic rays traverse a coherent field. Although this is not entirely accurate, the deflection of cosmic rays is taken into account by applying a magnetic lens. The second assumption is that the cosmic rays are of the same species. Finally, it is assumed that these cosmic rays originate from a source capable of producing multiple observable events.

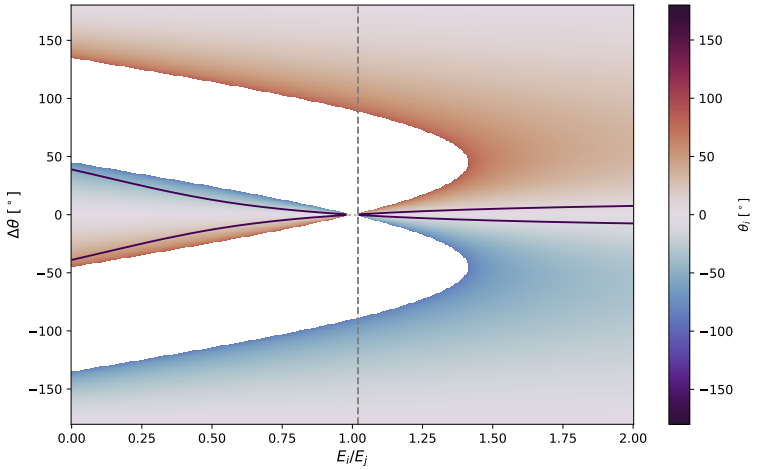

Figure 5.5: This graph shows for which values θ_j is less than a specific value. The white shade of the graph shows where the formalism function is invalid. The dotted line shows the restriction applied for the reduced energy Oikonomou et al. [10] suggested.

In addition to the assumptions required for this formalism to be valid, certain restrictions must be considered when calculating the multiplet pairs, this is to avoid unphysical pairs. The first constraint introduced is that the reduced energy must exceed $E_i/E_j > 1.02$. This is due to the formalism being invalid for certain combinations of $\Delta\theta$ and E_i/E_j, as shown in Fig. 5.5. For values below 1.02, θ_j becomes negative, which is undesirable in this context. The combined angle is restricted to be $\theta_j < 15°$, which is a result of the galactic-field model and the extra-galactic magnetic field model of [76, 77] which shows that the deflection of ultra-high energy protons with energies above $E > 5.0 \cdot 10^{19}$ eV experience deflections less than 15° [10].

The foundation for the formalism has now been established. To ensure numerical accuracy and account for uncertainties in sampling the arrival directions and energies, the energies and arrival directions are re-sampled 1000 times.

When all the re-constructed source directions have been calculated for the valid multiplet pairs. All the source directions are binned to a Skymap. For one iteration,

a top-hat filter is applied to the source directions with a degree of 5°. This is to find the largest cluster of reconstructed source directions.

5.3 Clustering Analysis applied on the Multiplet Search

Sky locations with many reconstructed source directions are potential sites of the cosmic-ray sources. The pixel with the highest number of source directions is located using the smoothed map with the top-hat filter. The pixel is converted to a specific position, which becomes the cluster's centre point. A region of 15° around the centre point is excluded from the rest of the map. In this region, the number of UHECR are counted. Having assumed earlier that a mutliplet pair of cosmic rays must lie within an area of 15° to each other for them to originate from the same source. When counting cosmic rays within each exclusion region, a region containing a UHECR source should have a higher cosmic ray count than a simulated background.

This algorithm has been executed approximately 100 times to ensure robustness and to mimic real events, accounting for the uncertainties in observations conducted by the Auger Observatory. The simulated cosmic rays are re-sampled 1000 times for both energies and positions. Each re-sampling yields slightly different positions, thereby incorporating observational uncertainties. This process also considers the randomness of background noise and the deflection effects of the extra-galactic magnetic field. This extensive sampling ensures sufficient data to distinguish a source or sources from the background statistically.

This clustering analysis can extend to finding several clusters of reconstructed source directions, but the thesis focuses on a simple scenario of one cluster.

Chapter 6

Results

This chapter will examine the potential of the method outlined in Chapter 5 for identifying UHECR sources. This section will present the results, including the statistical findings. The simulation is conducted by varying the declination of the source position to find to which degree the exposure and magnetic field contribute to observing a source position at a specific declination.

6.1 Pure Nitrogen Composition

Background Simulation

The simulated background is intended to resemble numerous weak, faint sources that collectively contribute to the observed isotropic distribution on Earth. Since this view is limited to the Southern Hemisphere, this simulation will only look at 1000 cosmic rays, with the simulation covering the entire sky. For the simulation to be similar to observed data from the Auger Observatory, the assumed amount of observed cosmic rays will be 70% of what is simulated. The cosmic rays in the background simulation will cover an energy range from $3.2{\cdot}10^{19}\,\mathrm{eV} < E < 1{\cdot}10^{22}\,\mathrm{eV}$. The source cosmic rays will also follow the same energy range, which will be discussed later. The spectral index utilized is $\gamma = -4.7$.

In this scenario, the background is composed entirely of nitrogen. To ensure a robust statistical analysis, the simulation was run 100 times. This repetition ensures that the collected data is sufficient for reliable statistical conclusions. The background simulation is anticipated to follow a Gaussian distribution, as observed in Fig. 6.1. By running the simulation 100 times, the calculated source direction is expected to appear at random positions. Given the uniform distribution of cosmic rays, the inclusion region generally contains some cosmic rays. When comparing the histogram of the background simulation to one with an added source, the background simulation is expected to show fewer instances with a high number of cosmic rays associated with the reconstructed source. The expected results of the background simulation are illustrated in Fig. 6.1.

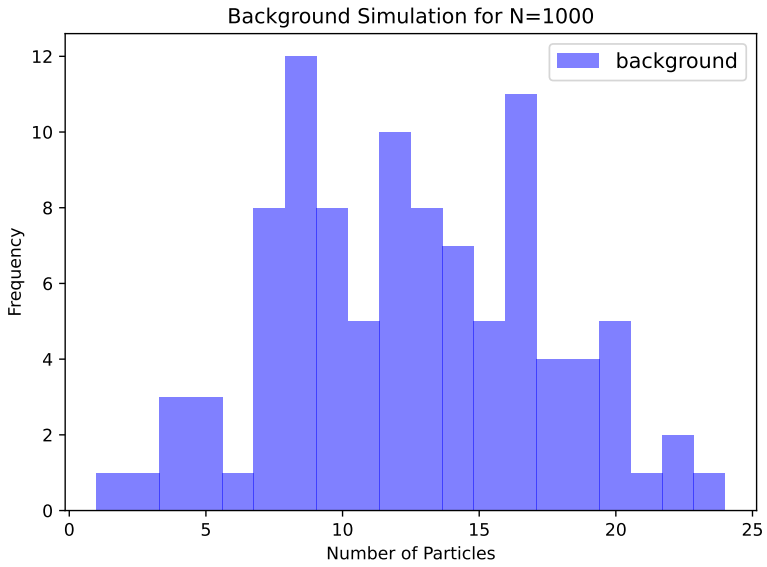

Figure 6.1: Histogram of the number of cosmic rays within a region of 15°, where the preformed algorithm has been conducted on a background model.

Examining the distribution of reconstructed source directions from the background simulation across the sky helps identify where the density is highest. Fig. 6.2 presents a graph showing the reconstructed source directions for the background, smoothed with a top-hat filter at 5° This figure aligns with our expectations: the reconstructed source directions are highly concentrated at lower declinations. This effect is due to the simulated view of the Auger Observatory, which has a clear view of declinations near the South Pole. Consequently, more cosmic rays are observed in this region, leading to a higher density of reconstructed source directions.

The effect of changing the source declination

A simulated source with a fixed number of cosmic rays is added to the simulation, reducing the number of cosmic rays in the background so that the total number of cosmic rays in the sky remains at 1000. This simulation aims to determine the declination and the number of UHECRs at which the overlap between the simulated background and the simulated source with background is less than 10%. When the overlap is $< 10\%$, the observed flux of cosmic rays is most guaranteed from a source. In this simulation, the number of cosmic rays from the source is fixed at N_{source} but changes the declination. The algorithm will run for four different declinations, $\delta = -20°, -40°, -60°, -80°$.

The background is simulated with 1000 nuclei, but the applied exposure ensures we only observe 70% of the simulated cosmic rays. This value was determined by calculating the approximate average of surviving cosmic rays following the applied exposure. We aim to determine if it is possible to distinguish a source from the observed background cosmic rays.

The source consists of 20 cosmic rays ($\sim 4\%$) and showed an overlap section for all declinations $> 63.0\%$. This implies that the source must be stronger to be detected using this approach. We next aim to determine if it is possible to distinguish a

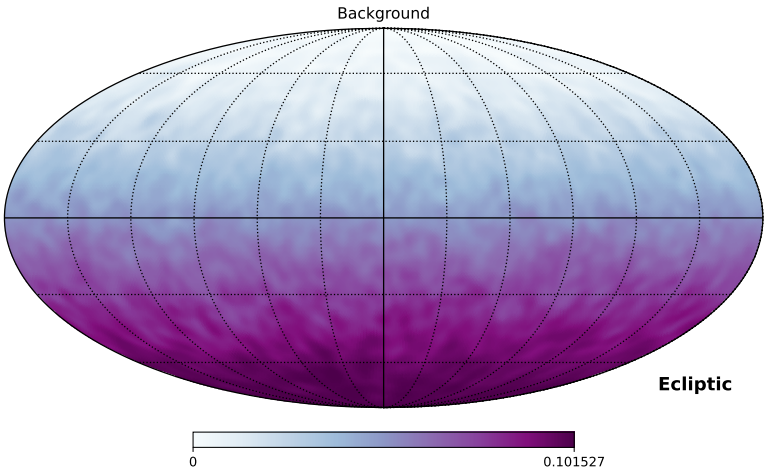

Figure 6.2: The skymap shows the reconstructed source direction for the background simulation with 1000 background cosmic rays, ran for 100 iterations.

source when it is only $\sim 30\%$ of the simulated background cosmic rays.

The energy distribution of the source cosmic rays assumes a spectral index of $\gamma = -2.0$. Assuming that the simulated source is nearby, the chosen spectral index is higher, making the spectrum less steep. For the chosen spectral index, we assume that the source is located in the distance of $\sim 20\,\mathrm{Mpc}$. Sources such as Cen A ($3-4\,\mathrm{Mpc}$) [78] and Fornax A ($\sim 22\,\mathrm{Mpc}$) [79] is lying close proximity to our Galaxy, and assuming that the possible source is nearby can be a good first approach.

The source's spectral index is distinctly different from the background because it is assumed that cosmic rays from the source contribute to a lower flux at lower energy bins, but more cosmic rays will reach higher energies compared to the background. Additionally, assuming the source is nearby, the spectral index is relatively hard due to reduced propagation effects.

Fig. 6.3 displays histograms depicting the overlap between the simulated background and an added source against the background. The different panels illustrate a source positioned at various declinations. The overlapping sections indicate the degree to which the source can be distinguished from the background. This source contributes $\sim 30\%$ of the total number of simulated cosmic rays. For this relative source strength, only sources located at declinations of $-80°$ are distinguishable from the background. The overlapping section for this source is 5%, indicating that it can be easily detected. However, when the source is positioned at higher declinations, such as $\delta = -60°$, it cannot be distinguished from the background, with an overlapping section of 22.1%. At even higher declinations, such as $\delta = -40°$ and $\delta = -20°$, the overlapping section exceeds 35%. This is likely due to a decreasing exposure of the Observatory at these declinations. This means that a source near the South Pole can be less luminous than sources at higher declinations and still be observed using this multiplet search method.

Looking at the trend line in Fig. 6.4 shows that the percentage overlap flattens out slightly at higher declinations, indicating that distinguishing a source at $\delta = -20°$

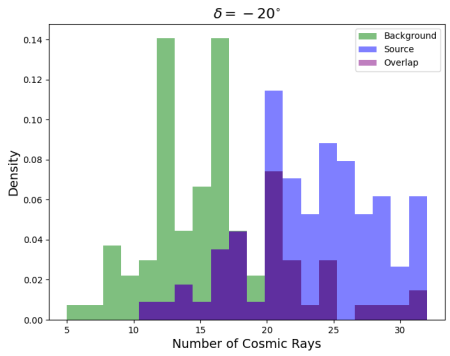

(a) The overlap section is 41.9%.

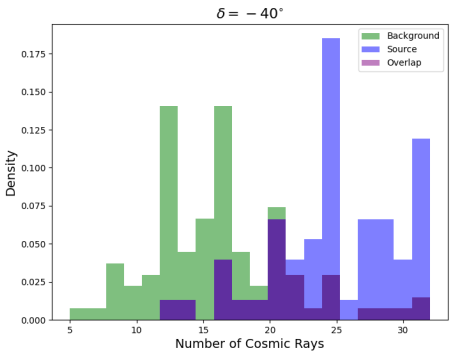

(b) The overlap section is 35.4%.

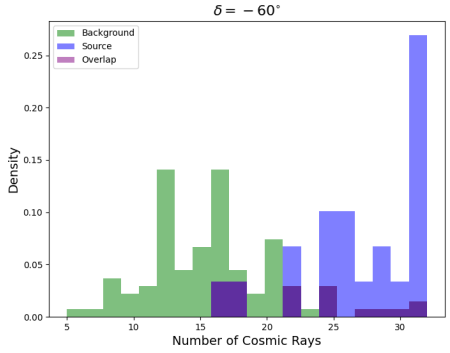

(c) The overlap section is 22.1%.

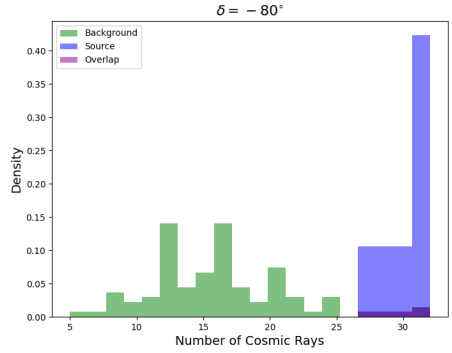

(d) The overlap section is 5.0%.

Figure 6.3: A simulated source is positioned at $\alpha = 100^\circ$ with a variable declination. This source has 210 simulated cosmic rays out of 1000 cosmic rays, all with a pure nitrogen composition.

and $\delta = -40^\circ$ that the number of cosmic rays for a source at these declinations may have a similar trend.

Simulate event similar to the Auger Observatory's database

Applying the simulation above to a realistic scenario to see how strong a source must be to detect it in the Auger Observatory's database. The minimum and maximum energy of the cosmic rays simulated are taken from the Auger Observatory's database of the 2600 most energetic events. The cosmic rays are simulated before the applied exposure of the Auger Observatory. By then, simulating a background of 4200 cosmic rays will give approximately 2600 cosmic rays remaining after the applied exposure. Since the simulation above with 1000 cosmic rays indicated that a source of strength 30% must be located at a declination of $\delta < -70^\circ$ to be detected, the source strength now consists of 10% of the background to see if it is possible to observe the source less strong.

The initial simulation was conducted with a source strength of 10% but did not yield any observable source. Following this, a source containing 1050 cosmic rays, approximately 25% of the simulated background, was added to evaluate if it can be distinguished from the background at any declination. This simulation randomly

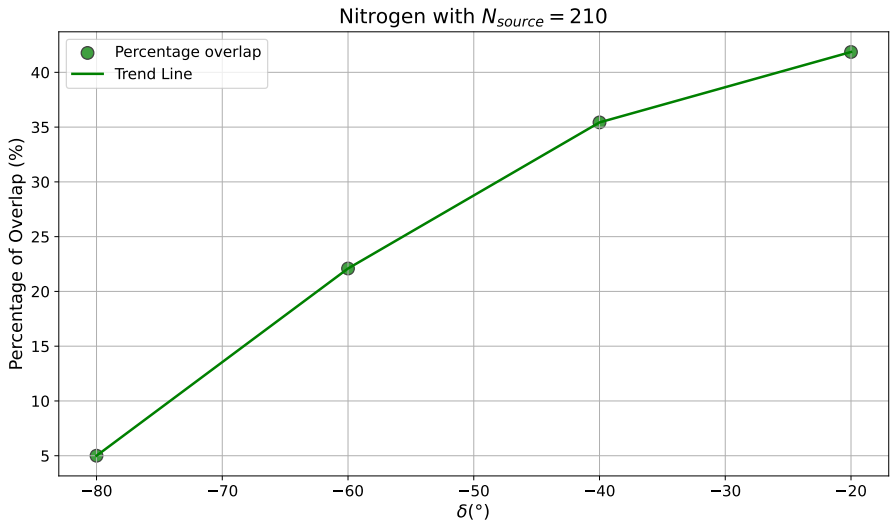

Figure 6.4: Shows the trend line for the percentage overlap at different declinations. For this simulation, the source is fixed at a certain right ascension.

selects the right ascension for each iteration, resulting in an average over all the right ascensions. The outcome demonstrates that choosing an arbitrary right ascension does not significantly affect the result. The results shown in Fig. 6.6 indicate that the source is distinguishable at all declinations.

The simulation indicates that all sources are detectable at the tested declinations. However, the source is more prominent at lower declinations, specifically at $\delta = -80°$ and $\delta = -60°$, where the overlap section is less than 2%. A source contributing 25% of the background is considered strong, as evidenced by the overlapping sections. This demonstrates that the method is quite powerful and capable of distinguishing strong sources at high declinations.

A source that produces 25% of the total emissivity on the GZK-volume must be at most $\delta = -20°$ to distinguish it from the background.

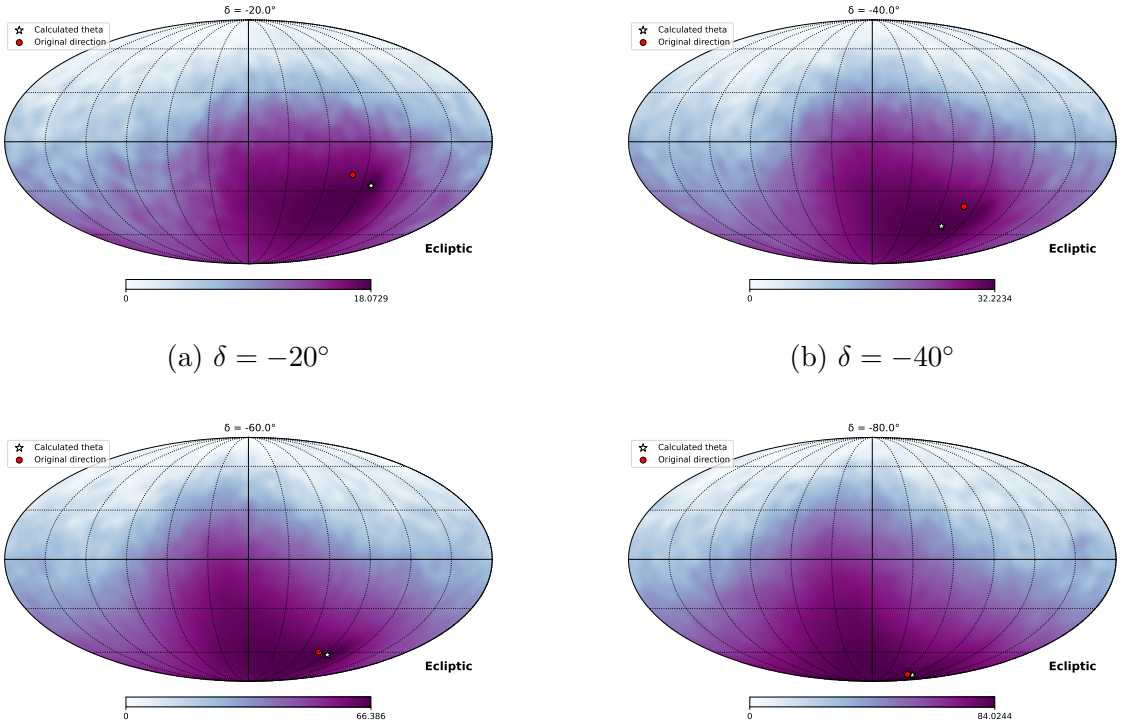

(a) $\delta = -20°$

(b) $\delta = -40°$

(c) $\delta = -60°$

(d) $\delta = -80°$

Figure 6.5: Smoothed map with 5000 cosmic rays. The red circle denotes the centre of the modelled source, and the white star shows the reconstructed source direction, denoted as theta in this plot.

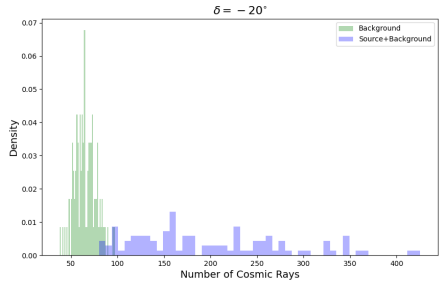

(a) The overlap section is 4.0%.

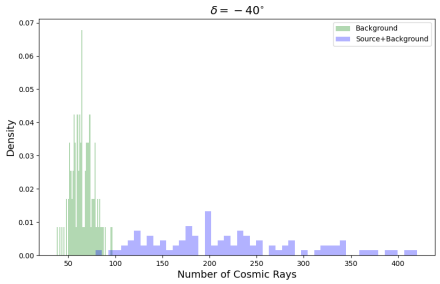

(b) The overlap section is 5.0%.

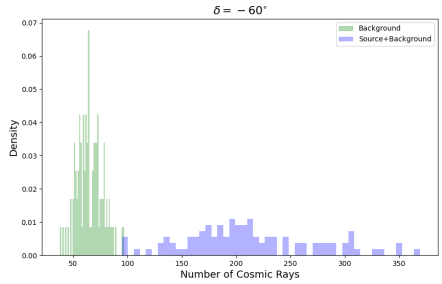

(c) The overlap section is 2.0%.

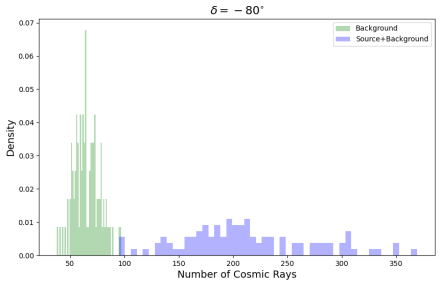

(d) The overlap section is 1.0%.

Figure 6.6: The panel shows the histograms representing the background and background with a simulated source for a source with 1050 cosmic rays and a background of 4200 cosmic rays.

Chapter 7

Further Work

This chapter will explore the algorithm's additional capabilities. This simulation aims to identify the strength at specific declinations where a source can be distinguished from the background. This information will then be applied to the Auger Observatory dataset, focusing on the 2600 most energetic events.

The multiplet formalism can also be extended to identify multiple clusters of high-density source directions. By varying the number of simulated sources, one can determine how many faint sources are required and the intensity at which they begin to resemble background noise.

The formalism can also be applied to different species of UHECR to see how the magnetic fields affect the arrival directions of cosmic rays. Since little is known about the composition of these cosmic rays, seeing how different species behave can possibly show a trend that can hopefully be seen in observed events.

An alternative approach for this specific algorithm is to execute it for additional iterations to reduce the uncertainties. The results obtained in this master's work exhibit trends similar to those expected from previous simulations. However, further reducing the uncertainties in the simulation would yield even more precise results. An additional feature that will improve the results is to look at what happens when a source is but at the boundary of the exposure to see if this will affect the results

With this algorithm, it is also possible to simulate a source that points towards the direction of a catalogued potential source such as Cen A or Fornax A. It would be interesting to see how the GMF will contribute to the deflection of these cosmic rays.

Chapter 8

Conclusion

Conducting a multiplet search on a simulated source against a background of 4200 cosmic rays necessitates that the source be 25% as strong as the background to be detectable at all declinations. The source must be significantly stronger at higher declinations to be distinguishable from the background for a weaker background. Moreover, the exposure of the Auger Observatory significantly impacts the outcomes of both simulations and observations. The varying ability to observe different regions of the sky substantially influences the required strength of the source, particularly in the context of the multiplet search.

In future applications of this search method, the algorithm can be expanded to analyze multiple sources. This will help determine the number of sources needed and the required strength of these sources to observe when they begin to blend into the background simulation.

This search method can also be applied to reconstruct a source at the observed location of known catalogued sources such as Cen A. By doing so, one can find out how strong the source must be to be observed at that certain point in the sky. Another possible approach with this search method is to expand it for more complicated compositions, as this is a more realistic scenario.

Bibliography

[1] Resconi Gaisser Engel. *Cosmic Rays and Particle Physics. Second Edition.* 2016.

[2] *Victor Hess discovers cosmic rays.* CERN. URL: https://timeline.web.cern.ch/victor-hess-discovers-cosmic-rays-0 (visited on 08/04/2024).

[3] John Linsley. 'Evidence for a Primary Cosmic-Ray Particle with Energy 10^{20} eV'. In: *Phys. Rev. Lett.* 10 (4 Feb. 1963), pp. 146–148. DOI: 10.1103/PhysRevLett.10.146. URL: https://link.aps.org/doi/10.1103/PhysRevLett.10.146.

[4] Karl-Heinz Kampert and Peter Tinyakov. 'Cosmic rays from the ankle to the cutoff'. In: *Comptes Rendus. Physique* 15.4 (2014), pp. 318–328.

[5] Domenik Ehlert, Foteini Oikonomou and Michael Unger. 'Curious case of the maximum rigidity distribution of cosmic-ray accelerators'. In: *Physical Review D* 107.10 (2023), p. 103045.

[6] Pierre Auger Collaboration. *Where do the most energetic particles in the universe come from?* Pierre Auger Observatory. 8-04-2024. URL: https://www.auger.org/news/scientific-highlights/311-where-do-the-most-energetic-particles-in-the-universe-come-from.

[7] Telescope Array. *Telescope Array Project: Home.* TA. 23-04-2024. URL: http://www.telescopearray.org/.

[8] Manlio De Domenico et al. 'Reinterpreting the development of extensive air showers initiated by nuclei and photons'. In: *Journal of Cosmology and Astroparticle Physics* 2013.07 (2013), p. 050.

[9] Alexander Aab et al. 'Search for magnetically-induced signatures in the arrival directions of ultra-high-energy cosmic rays measured at the Pierre Auger Observatory'. In: *Journal of Cosmology and Astroparticle Physics* 2020.06 (2020), p. 017.

[10] Foteini Oikonomou and Miguel Mostafa. 'A Magnetic spectrometer analysis of ultra high energy cosmic ray arrival directions'. In: *PoS, ICRC2017* 525 (2018).

[11] Miguel Molero Gonzalez. 'Measurement of the Cosmic Ray Anisotropy with AMS-02 on the International Space Station'. PhD thesis. Centro de Investigaciones Energéti cas Medioambientales y Tecnológicas (ES), 2021.

[12] Anthony M Hillas. 'The origin of ultra-high-energy cosmic rays'. In: *Annual review of astronomy and astrophysics* 22.1 (1984), pp. 425–444.

[13] Dirk Kickelbick. 'The energy spectrum of primary cosmic rays measured with the KASCADE-Grande experiment'. In: (2008).

[14] Paolo Lipari. 'Spectral features in the cosmic ray fluxes'. In: *Astroparticle Physics* 97 (2018), pp. 197–204.

[15] Pierre Auger Observatory. *Catalog dataset*. 2019. URL: https://opendata.auger.org/catalog/index.php?evid=191110#display (visited on 28/04/2024).

[16] G Matthiae and V Verzi. 'The energy spectrum of cosmic rays at very high energy'. In: *La Rivista del Nuovo Cimento* 38 (2015), pp. 73–132.

[17] Kenneth Greisen. 'End to the cosmic-ray spectrum?' In: *Physical Review Letters* 16.17 (1966), p. 748.

[18] G. T. Zatsepin and V. A. Kuzmin. 'Upper limit of the spectrum of cosmic rays'. In: *JETP Lett.* 4 (1966), pp. 78–80.

[19] Darko Veberic. 'The end of the cosmic ray spectrum'. In: *arXiv preprint arXiv:1110.0615* (2011).

[20] Dietrich Müller. 'The composition of cosmic rays at high energies'. In: *Advances in space research* 9.12 (1989), pp. 31–43.

[21] Alexey Yushkov, Pierre Auger Collaboration et al. 'Mass Composition of Cosmic Rays with Energies above 10{17.2} eV from the Hybrid Data of the Pierre Auger Observatory'. In: *36th International Cosmic Ray Conference*. Vol. 358. Sissa Medialab. 2021, p. 482.

[22] RU Abbasi et al. 'Depth of ultra high energy cosmic ray induced air shower maxima measured by the telescope array black rock and long ridge FADC fluorescence detectors and surface array in hybrid mode'. In: *The Astrophysical Journal* 858.2 (2018), p. 76.

[23] M Bustamante et al. 'High-energy cosmic-ray acceleration'. In: (2010).

[24] Alexander Aab et al. 'Cosmic-ray anisotropies in right ascension measured by the Pierre Auger Observatory'. In: *The Astrophysical Journal* 891.2 (2020), p. 142.

[25] Alexander Aab et al. 'Search for patterns by combining cosmic-ray energy and arrival directions at the Pierre Auger Observatory'. In: *The European Physical Journal C* 75 (2015), pp. 1–15.

[26] Pierre Auger Collaboration et al. 'Observation of a large-scale anisotropy in the arrival directions of cosmic rays above 8× 1018 eV'. In: *Science* 357.6357 (2017), pp. 1266–1270.

[27] A Abdul Halim et al. 'Constraining models for the origin of ultra-high-energy cosmic rays with a novel combined analysis of arrival directions, spectrum, and composition data measured at the Pierre Auger Observatory'. In: *Journal of Cosmology and Astroparticle Physics* 2024.01 (2024), p. 022.

[28] Joao de Mello Neto. 'Physics and astrophysics of ultra-high energy cosmic rays: recent results from the Pierre Auger Observatory'. In: *arXiv preprint arXiv:2012.12943* (2020).

[29] Jorge Abraham et al. 'The fluorescence detector of the Pierre Auger Observatory'. In: *Nuclear Instruments and Methods in Physics Research Section A: Accelerators, Spectrometers, Detectors and Associated Equipment* 620.2-3 (2010), pp. 227–251.

[30] Rafael Alves Batista et al. 'Open questions in cosmic-ray research at ultrahigh energies'. In: *Frontiers in Astronomy and Space Sciences* 6 (2019), p. 23.

[31] Petr Nečesal, forthe Pierre Auger Collaboration et al. 'The fluorescence detector of the pierre auger observatory'. In: *Journal of Physics: Conference Series*. Vol. 293. 1. IOP Publishing. 2011, p. 012036.

[32] Roberto Aloisio. 'Acceleration and propagation of ultra-high energy cosmic rays'. In: *Progress of Theoretical and Experimental Physics* 2017.12 (2017), 12A102.

[33] Enrico Fermi. 'On the origin of the cosmic radiation'. In: *Physical review* 75.8 (1949), p. 1169.

[34] Matthew G Baring. 'Diffusive shock acceleration of high energy cosmic rays'. In: *Nuclear Physics B-Proceedings Supplements* 136 (2004), pp. 198–207.

[35] AR Bell et al. 'Cosmic-ray acceleration by relativistic shocks: limits and estimates'. In: *Monthly Notices of the Royal Astronomical Society* 473.2 (2018), pp. 2364–2371.

[36] Maurizio Spurio. *Particles and Astrophysics. A Multi-Messenger Approach*. 2015.

[37] Dimitrios Giannios. 'UHECRs from magnetic reconnection in relativistic jets'. In: *Monthly Notices of the Royal Astronomical Society: Letters* 408.1 (2010), pp. L46–L50.

[38] Maxim Lyutikov and Rachid Ouyed. 'Inductive acceleration of UHECRs in sheared relativistic jets'. In: *Astroparticle Physics* 27.6 (2007), pp. 473–489.

[39] Michael Kachelriess. 'Extragalactic cosmic rays'. In: *arXiv preprint arXiv:2201.04535* (2022).

[40] RD Blandford. 'Acceleration of ultra high energy cosmic rays'. In: *Physica Scripta* 2000.T85 (2000), p. 191.

[41] The Open University. *Introduction to Active Galaxies*. URL: https://www.open.edu/openlearn/science-maths-technology/introduction-active-galaxies/content-section-1 (visited on 09/05/2022).

[42] Paolo Padovani. 'On the two main classes of active galactic nuclei'. In: *Nature Astronomy* 1.8 (2017), p. 0194.

[43] Frank M Rieger. 'Active Galactic Nuclei as Potential Sources of Ultra-High Energy Cosmic Rays'. In: *Universe* 8.11 (2022), p. 607.

[44] NASA. *Bright Galaxy Centaurus A*. 2014. URL: https://www.nasa.gov/image-article/bright-galaxy-centaurus/ (visited on 07/05/2024).

[45] M. Koppitz and L. Rezzolla. *Gamma-ray Bursts*. 2013. URL: https://imagine.gsfc.nasa.gov/science/objects/bursts1.html (visited on 13/03/2024).

[46] Kohta Murase and Imre Bartos. 'High-energy multimessenger transient astrophysics'. In: *Annual Review of Nuclear and Particle Science* 69 (2019), pp. 477–506.

[47] Mario Vietri. 'On the acceleration of ultra high energy cosmic rays in gamma ray bursts'. In: *arXiv preprint astro-ph/9506081* (1995).

[48] B Theodore Zhang et al. 'Low-luminosity gamma-ray bursts as the sources of ultrahigh-energy cosmic ray nuclei'. In: *Physical Review D* 97.8 (2018), p. 083010.

[49] Glennys R Farrar and Tsvi Piran. 'Tidal disruption jets as the source of Ultra-High Energy Cosmic Rays'. In: *arXiv preprint arXiv:1411.0704* (2014).

[50] Tsvi Piran and Paz Beniamini. 'Ultra high energy cosmic rays from tidal disruption events'. In: *Journal of Cosmology and Astroparticle Physics* 2023.11 (2023), p. 049.

[51] Valenti Bosch-Ramon. 'The role of supernovae inside AGN jets in UHECR acceleration'. In: *Astronomy & Astrophysics* 677 (2023), p. L14.

[52] David Moss et al. 'Multiscale magnetic fields in spiral galaxies: evolution and reversals'. In: *Astronomy & Astrophysics* 537 (2012), A68.

[53] Ronnie Jansson and Glennys R Farrar. 'The galactic magnetic field'. In: *The Astrophysical Journal Letters* 761.1 (2012), p. L11.

[54] Glennys R Farrar. 'The Galactic magnetic field and ultrahigh-energy cosmic ray deflections'. In: *Comptes Rendus. Physique* 15.4 (2014), pp. 339–348.

[55] Michael Unger and Glennys Farrar. 'The Coherent Magnetic Field of the Milky Way'. In: *arXiv preprint arXiv:2311.12120* (2023).

[56] J Tjemsland, M Meyer and F Vazza. 'Constraining the astrophysical origin of intergalactic magnetic fields'. In: *arXiv preprint arXiv:2311.04273* (2023).

[57] Glennys R Farrar and Michael S Sutherland. 'Deflections of UHECRs in the Galactic magnetic field'. In: *Journal of Cosmology and Astroparticle Physics* 2019.05 (2019), p. 004.

[58] Janning Meinert et al. 'Modified temperature redshift relation and UHECR propagation'. In: *arXiv preprint arXiv:2309.08451* (2023).

[59] The Kavli Foundation. *Cosmic Microwave Background*. 2024. URL: https://kipac.stanford.edu/research/topics/cosmic-microwave-background (visited on 11/05/2024).

[60] RC Gilmore et al. 'Semi-analytic modeling of the EBL and consequences for extragalactic gamma-ray spectra https://doi. org/10.1111/j. 1365-2966.2012. 20841. x Mon'. In: *Not. Roy. Astron. Soc* 422.3189 (2012), pp. 1104–0671.

[61] MT Dova. 'Ultra-high energy cosmic rays'. In: *arXiv preprint arXiv:1604.07584* (2016).

[62] R Alves Batista et al. 'Effects of uncertainties in simulations of extragalactic UHECR propagation, using CRPropa and SimProp'. In: *Journal of Cosmology and Astroparticle Physics* 2015.10 (2015), p. 063.

[63] Shigeru Yoshida and Masahiro Teshima. 'Energy spectrum of ultra-high energy cosmic rays with extra-galactic origin'. In: *Progress of theoretical physics* 89.4 (1993), pp. 833–845.

[64] Rafael Alves Batista, Peter Schiffer and Günter Sigl. 'Propagation of UHECRs in the universe'. In: *Nuclear Instruments and Methods in Physics Research Section A: Accelerators, Spectrometers, Detectors and Associated Equipment* 742 (2014), pp. 245–249.

[65] Alexander Aab et al. 'Combined fit of spectrum and composition data as measured by the Pierre Auger Observatory'. In: *Journal of Cosmology and Astroparticle Physics* 2017.04 (2017), p. 038.

[66] Georgy I Burde. 'Particle dynamics and GZK limit in relativity with a preferred frame'. In: *Astroparticle Physics* 126 (2021), p. 102526.

[67] Christopher Heiter et al. 'Production and propagation of ultra-high energy photons using CRPropa 3'. In: *Astroparticle Physics* 102 (2018), pp. 39–50.

[68] R Alves Batista et al. 'CRPropa: a public framework to propagate UHECRs in the universe'. In: *Epj web of conferences*. Vol. 99. EDP Sciences. 2015, p. 13004.

[69] E Kido et al. 'Evaluations of uncertainties in simulations of propagation of ultrahigh-energy cosmic-ray nuclei derived from microscopic nuclear models'. In: *Astroparticle Physics* 152 (2023), p. 102866.

[70] Floyd William Stecker. 'Photodisintegration of ultrahigh-energy cosmic rays by the universal radiation field'. In: *Physical Review* 180.5 (1969), p. 1264.

[71] Oleg Kalashev, Maxim Pshirkov and Mikhail Zotov. 'Analysing arrival directions of ultra-high-energy cosmic rays with convolutional neural networks'. In: *Journal of Physics: Conference Series*. Vol. 2438. 1. IOP Publishing. 2023, p. 012067.

[72] Eli Waxman and Jordi Miralda-Escude. 'Images of bursting sources of high-energy cosmic rays: effects of magnetic fields'. In: *The Astrophysical Journal* 472.2 (1996), p. L89.

[73] Rafael Alves Batista et al. 'CRPropa 3—a public astrophysical simulation framework for propagating extraterrestrial ultra-high energy particles'. In: *Journal of Cosmology and Astroparticle Physics* 2016.05 (2016), p. 038.

[74] Alexander Aab et al. 'Features of the energy spectrum of cosmic rays above 2.5× 10 18 eV using the pierre auger observatory'. In: *Physical review letters* 125.12 (2020), p. 121106.

[75] Paul Sommers. 'Cosmic ray anisotropy analysis with a full-sky observatory'. In: *Astroparticle Physics* 14.4 (2001), pp. 271–286.

[76] Ronnie Jansson and Glennys R Farrar. 'A new model of the galactic magnetic field'. In: *The Astrophysical Journal* 757.1 (2012), p. 14.

[77] MS Pshirkov et al. 'Deriving the global structure of the galactic magnetic field from Faraday rotation measures of extragalactic sources'. In: *The Astrophysical Journal* 738.2 (2011), p. 192.

[78] ESO. *Radio galaxy Centaurus A*. European Southern Observatory. 14-04-2024. URL: https://www.eso.org/public/images/eso0005b/.

[79] NASA. *The Dusty Galaxy NGC 1316*. URL: https://hubblesite.org/contents/media/images/2005/11/1671-Image.html (visited on 29/05/2024).

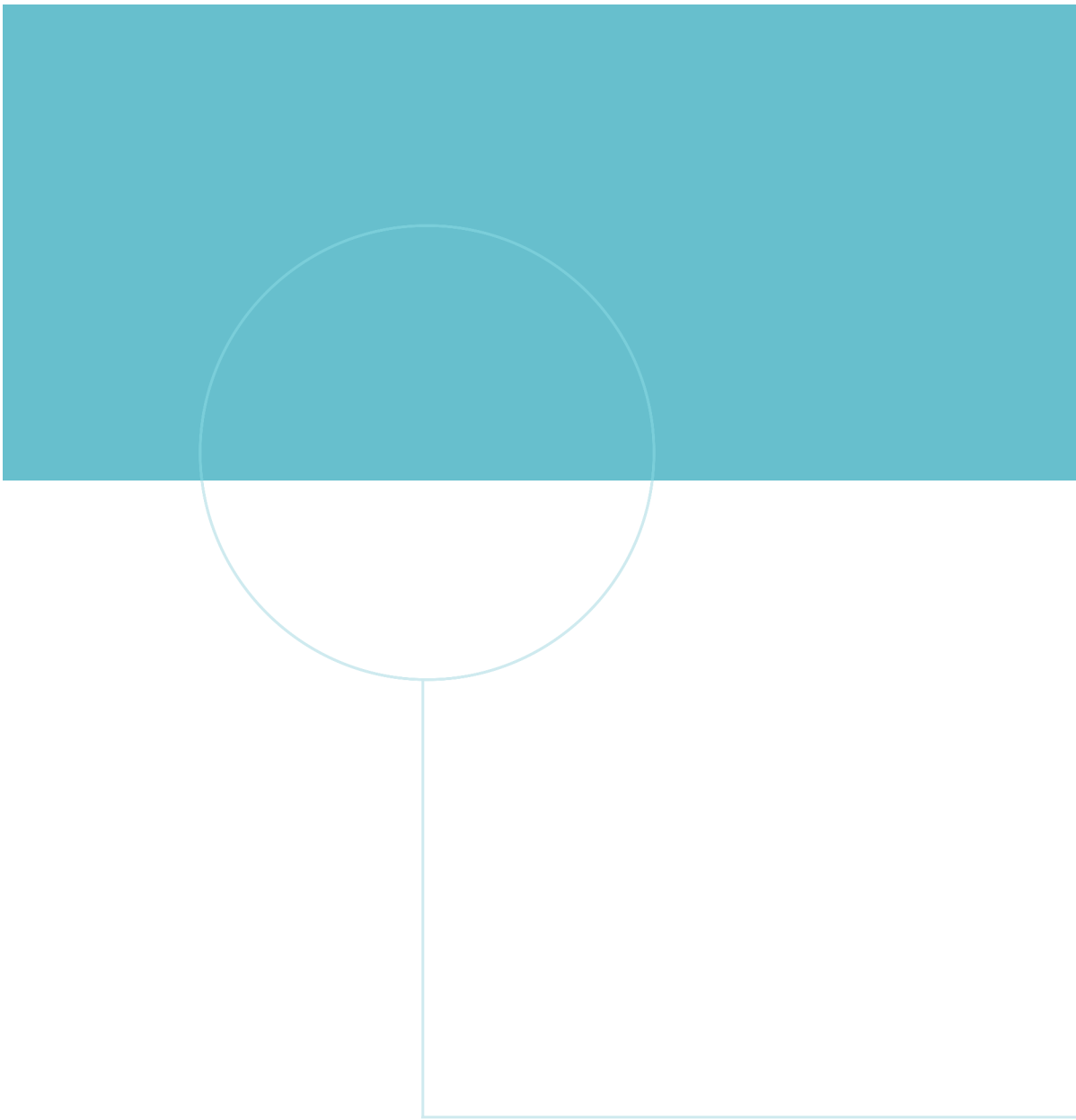

NTNU

Norwegian University of
Science and Technology